

What is the mechanism of power-law distributed Poincaré recurrences in higher-dimensional systems?

Steffen Lange,¹ Arnd Bäcker,^{1,2} and Roland Ketzmerick^{1,2}

¹*Technische Universität Dresden, Institut für Theoretische Physik and Center for Dynamics, 01062 Dresden, Germany*

²*Max-Planck-Institut für Physik komplexer Systeme, Nöthnitzer Straße 38, 01187 Dresden, Germany*

(Dated: March 3, 2022)

The statistics of Poincaré recurrence times in Hamiltonian systems typically shows a power-law decay with chaotic trajectories sticking to some phase-space regions for long times. For higher-dimensional systems the mechanism of this power-law trapping is still unknown. We investigate trapped orbits of a generic 4D symplectic map in phase space and frequency space and find that, in contrast to 2D maps, the trapping is (i) not due to a hierarchy in phase space. Instead, it occurs at the surface of the regular region, (ii) outside of the Arnold web. The chaotic dynamics in this sticky region is (iii) dominated by resonance channels which reach far into the chaotic region: We observe (iii.a) clear signatures of some kind of partial transport barriers and conjecture (iii.b) a stochastic process with an effective drift along resonance channels. These two processes lay the basis for a future understanding of the mechanism of power-law trapping in higher-dimensional systems.

Chaotic transport in Hamiltonian systems is of great importance in a wide variety of applications, e.g., for predicting the stability of celestial motion and satellites [1–3], controlling the beams of particle accelerators [4–7], and to describe the dynamics of atoms and molecules [8–13]. Generic Hamiltonian systems are not fully chaotic but have a mixed phase space which also contains regular tori. Close to these tori the chaotic transport is slowed down considerably. This intermittent behavior is characterized by the (cumulative) Poincaré recurrence statistics $P(t)$, the probability that a chaotic orbit has not returned to an initial region within time t . While for fully chaotic systems $P(t)$ usually decays exponentially [14, 15], for mixed systems the decay is much slower following a power law $P(t) \sim t^{-\gamma}$ [16, 17]. This so-called power-law trapping or stickiness entails dramatic consequences for the transport properties in many systems, e.g., comets in the solar system [18], reactant lifetime in transition state theory [19], DNA [20], intramolecular energy redistribution [21], and microwave ionization of Rydberg atoms [8, 22, 23].

Power-law trapping is well understood for Hamiltonian systems with two degrees of freedom [24–33]: In this case the regular tori are barriers in phase space such that chaotic orbits cannot cross them. In their vicinity so-called partial transport barriers of the same dimension exist which can be crossed by chaotic orbits, but with a small rate. A hierarchy of these partial barriers governs the dynamics and causes the power-law trapping.

Power-law trapping is also observed in higher-dimensional systems [35–39], see Fig. 1 for an illustration. However, its origin is unknown as the mechanism for two degrees of freedom cannot be generalized: The distinctive feature of higher-dimensional systems is that the regular tori have an insufficient dimension to be barriers in phase space (i.e. the f -dimensional tori have at least two dimensions less than the $(2f - 1)$ -dimensional energy surface for $f \geq 3$ degrees of freedom). Consequentially, any chaotic orbit can get arbitrarily close to

any regular torus by transport along resonance channels of the so-called Arnold web [40–42]. While the diffusion along a channel is sometimes found [43–45] and often assumed [46, 47] to be normal, its detailed understanding is still missing [42, 47, 48]. Generalizations of partial barriers to higher-dimensional systems exist [37, 49–51] but their relevance for the chaotic transport is unclear. The phenomenon of power-law trapping can be explained in weakly coupled systems for intermediate time-scales [36, 39]. Still, the generic mechanism of power-law trapping in higher-dimensional systems remains an open question.

In this paper we investigate the mechanism of power-

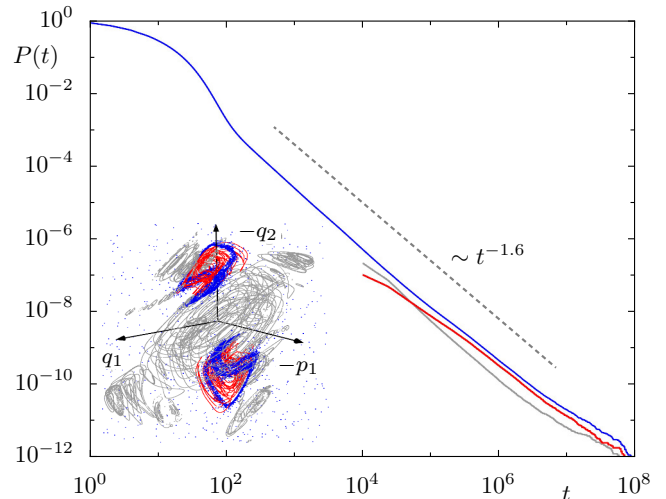


FIG. 1. Statistics of Poincaré recurrences $P(t)$ for the map (1) with initial region $q_1 < 0.1$ showing a power-law decay $P(t) \sim t^{-1.6}$. For $t > 10^4$ the statistics (blue) is decomposed into orbits trapped at the dominant sticky region (red) and the remainder (gray). The inset shows the 3D phase-space slice with $\vec{n} = (0, 1, 0, 0)$, $D = 0$ with a trapped orbit (blue points) and regular tori (red and gray rings). For a rotating view of the inset see the supplemental material [34].

law trapping in a generic 4D symplectic map, which corresponds to the lowest dimensional Hamiltonian system for which regular tori are no barriers in phase space. We find that the trapping is (i) not due to a hierarchy in phase space, in contrast to 2D maps. Moreover, it occurs at the surface of the regular region, (ii) outside of the Arnold web. We find that the chaotic dynamics in this sticky region is (iii) dominated by resonance channels, which extend out of the Arnold web far into the chaotic region: We demonstrate (iii.a) clear signatures of some kind of partial transport barriers for the transport across channels. We conjecture that (iii.b) a stochastic process with an effective drift models the transport along a channel. Determining which of these two processes is dominant should allow for unraveling the mechanism of power-law trapping in higher-dimensional Hamiltonian systems.

System and Poincaré recurrence statistics.— To study the power-law trapping for 4D maps, we consider two coupled standard maps [52], $(p_1, p_2, q_1, q_2) \mapsto (p'_1, p'_2, q'_1, q'_2)$,

$$q'_i = q_i + p_i \quad p'_i = p_i - \frac{\partial V_i}{\partial q_i}(q'_i) - \frac{\partial V_{12}}{\partial q_i}(q'_1, q'_2) \quad (1)$$

with potentials $V_i = K_i/(4\pi^2) \cos(2\pi q_i)$ and coupling $V_{12} = \xi_{12}/(4\pi^2) \cos(2\pi(q_1 + q_2))$. Choosing the non-linearity parameters $K_1 = 2.25$, $K_2 = 3.0$ and a large coupling parameter $\xi_{12} = 1.0$, Eq. (1) represents a generic 4D symplectic map far from integrability [53]. There is an elliptic–elliptic fixed point at $(p_1, p_2, q_1, q_2) = (0, 0, 0.5, 0.5)$ which is surrounded by regular tori. For a 4D map such regular tori are two-dimensional and are organized around families of elliptic 1D tori which form a hierarchy [54]. These regular structures are embedded in a large chaotic region. We obtain the statistics of Poincaré recurrences $P(t)$ for the map (1) in a phase space $p_{1,2} \in [-0.5, 0.5)$ and $q_{1,2} \in [0, 1)$ with periodic boundaries and the initial region $q_1 < 0.1$, which contains only chaotic dynamics. The resulting statistics $P(t)$ in Fig. 1 (solid blue line) exhibits a power-law decay over several orders of magnitude. Chaotic orbits with large recurrence times t stick to the vicinity of different regions of regular tori. As an illustration the 3D phase-space slice (explained below) in the inset in Fig. 1 shows regular tori (gray) and a chaotic orbit (blue) which sticks to a region of regular tori marked in red. It turns out that this sticky region is dominantly responsible for the power-law decay for $10^5 < t < 10^8$: The decomposition of $P(t)$ for $t > 10^4$ demonstrates that the fraction of orbits sticking to this region (red line) is much bigger than the rest (gray line). Thus, for the rest of the paper we focus on chaotic orbits trapped in this dominant sticky region.

Visualization in phase space and frequency space.— In order to analyze the mechanism of power-law trapping, we study the trapped orbits in phase space, using 3D phase-space slices [53], and frequency space. This is illustrated in Figs. 2(a) and (b), respectively, for a typical chaotic orbit (same as in the inset of Fig. 1) trapped in the dominant sticky region: For a 3D phase-space slice only points $\vec{u} = (p_1, p_2, q_1, q_2)$ within a thin 3D slice are

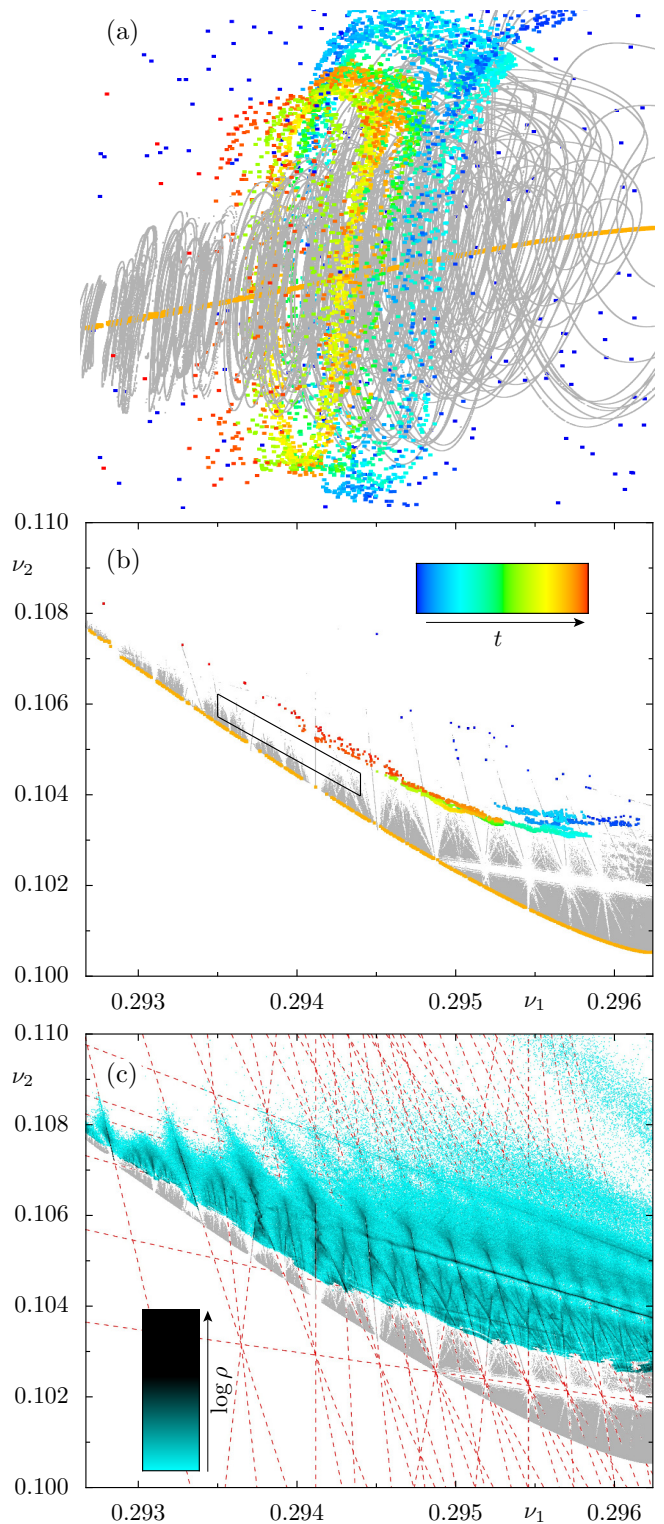


FIG. 2. Dominant sticky region in (a) 3D phase-space slice ($\vec{n} = (0.632, 0.611, 0.314, 0.359)$, $D = 0.322$) and (b), (c) frequency space with regular tori (gray) rings and (b), (c) points) and elliptic 1D tori (orange). In (a), (b) a single trapped orbit is shown with the time $t \in [0, 1.7 \cdot 10^7]$ encoded in color (blue to red). In (c) the density $\rho(\nu_1, \nu_2)$ of frequencies, see (ii), is shown with resonance lines (red). White corresponds to $\rho = 0$, turquoise to black to $\rho \in [4 \cdot 10^{-7}, 2 \cdot 10^{-3}]$. For a rotating view of (a) see the supplemental material [34].

displayed in the remaining three dimensions. The slice is defined by $|\vec{u} \cdot \vec{n} - D| < 10^{-4}$ with normal vector \vec{n} and distance D to the origin given in the captions of Fig. 1 and Fig. 2. Phase-space objects typically appear in such a slice with a dimension reduced by one. For instance the regular 2D tori appear as rings (gray) in Fig. 2(a) and the elliptic 1D tori appear as points (orange). Since elliptic 1D tori occur in one-parameter families around which the regular tori are organized [54], the orange points form a line in the center of the gray rings.

In order to relate trapped orbits to resonances, we complement the 3D phase-space slice with a frequency analysis [53, 55, 56], see Fig. 2(b): For this, each 2D torus is associated with its two fundamental frequencies $(\nu_1, \nu_2) \in [0, 1)^2$, i.e. a point in frequency space. The frequencies (ν_1, ν_2) describe the angular dynamics on the torus and are computed from $\Delta t = 4096$ iterations of an orbit on the torus. In the frequency space in Fig. 2(b) regular tori (gray points) are organized above the family of elliptic 1D tori (orange points). The region of the regular tori is interrupted by channels around resonance lines $m_1 : m_2 : n$, on which the frequencies fulfill $m_1 \cdot \nu_1 + m_2 \cdot \nu_2 = n$ with integers m_1, m_2, n . These so-called *resonance channels* are accessible to chaotic dynamics. Their network within the region of regular tori is referred to as *Arnold web*. A chaotic orbit can be displayed in frequency space by decomposing the orbit into segments of length Δt and numerically assigning frequencies to each segment [44, 49].

(i) *Trapping not due to hierarchy.*— A typical trapped orbit is shown in Figs. 2(a) and (b) with its points colored according to iteration time: The orbit enters the sticky region (blue), is trapped (bright blue to orange), and leaves the region (red). The 3D phase-space slice and the frequency space demonstrate that the chaotic orbit is not trapped deep in the hierarchy: In Fig. 2(a) the trapped orbit is spread over the surface of the regular structure without clustering on smaller scales. In contrast, trapped orbits in 2D maps spend more and more time on finer and finer phase-space scales due to the hierarchy of partial barriers. Furthermore, in Fig. 2(b) the orbit extends over several resonances, whereas an orbit being trapped in the deeper levels of the island-around-island hierarchy of a 4D map would have frequencies on a single resonance line or at a junction of resonances [54]. We estimate that the trapped orbits spend on average just 1% of their time deeper in the hierarchy, e.g. near those regular tori which appear on resonance lines in Fig. 2(b).

(ii) *Trapping outside of Arnold web.*— We analyze all trapped orbits with $10^5 < t < 10^9$ using their density $\rho(\nu_1, \nu_2)$ in frequency space, see Fig. 2(c). The density is computed from 61600 trapped orbits on a grid with resolution $\Delta\nu = 5 \cdot 10^{-6}$ and shown in logarithmic scale. The density is zero in the resonance channels of the Arnold web. This means that on the considered time scale the power-law trapping occurs outside of the Arnold web.

(iii) *Relevance of resonance channels.*— Remarkably, the density in Fig. 2(c) exhibits pronounced peaks along

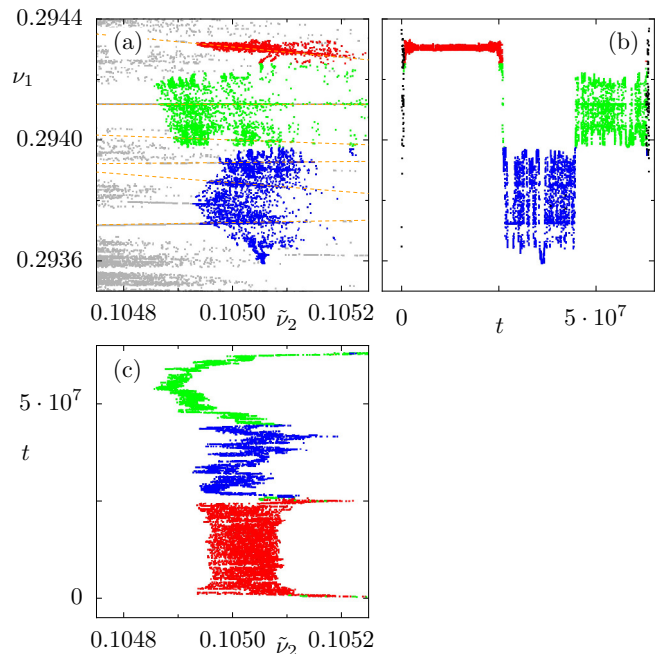


FIG. 3. Transport across and along resonance channels for a single trapped orbit $t \in [0, 6.3 \cdot 10^7]$ displayed in local coordinates $(\nu_1, \tilde{\nu}_2)$ with $\tilde{\nu}_2 = \nu_2 + k \cdot (\nu_1 - \nu_1^0)$, $k = 1.94$, $\nu_1^0 = 0.294$. The boundary of (a) is indicated as a black box in Fig. 2(b). Different frequency ranges in ν_1 are colored red, green and blue. In (b), (c) the time dependence of ν_1 (across) and $\tilde{\nu}_2$ (along) is shown (points outside of (a) in black).

resonance lines, some of which are indicated by red dashed lines in the background. These resonance lines extend out of the Arnold web into the chaotic region. For a chaotic orbit to exhibit resonant frequencies it has to be confined around a resonance line at least for the time interval Δt of the frequency analysis. This would be the case within resonance channels in the Arnold web, where they are surrounded by regular tori. The high densities in Fig. 2(c) demonstrate that these resonance channels still dominate transport outside the Arnold web, where they are no longer surrounded by regular tori. Consequently, the chaotic transport in the sticky region can locally be decomposed into transport across and along resonance channels.

In Fig. 3 this decomposition is demonstrated for a trapped orbit by using convenient local coordinates $(\nu_1, \tilde{\nu}_2)$. The boundary of Fig. 3(a) is shown as black box in Fig. 2(a). The transport across and along resonance channels is captured by $\nu_1(t)$ in Fig. 3(b) and $\tilde{\nu}_2(t)$ in Fig. 3(c), respectively, as discussed below. Note that, while most trapped orbits extend much more along ν_1 than the example orbit, locally we always observe the characteristics of Fig. 3.

(iii.a) *Signatures of partial barriers.*— The transport across resonance channels is captured in Fig. 3(b). The frequency $\nu_1(t)$ fluctuates within some frequency range over long time intervals with sudden transitions to other

ranges. In 2D maps such behavior is caused by partial barriers [57]. Thus, Fig. 3(b) shows clear signatures of partial barriers separating one or more resonance channels in a generic 4D map.

The origin of these partial barriers is a difficult open problem: Partial barriers can be formed by the stable and unstable manifolds of the family of hyperbolic 1D tori, which is present in any resonance channel [58] and studied in the context of normally hyperbolic invariant manifolds [50]. Instead, we conjecture that the partial barriers are formed by some families of cantori, as they occur in Fig. 3(a) in between resonance channels. The existence of individual cantori in higher dimensions has been shown in Ref. [51]. The quantification of the flux across such a partial barrier in higher-dimensional systems is conceptually problematic: As the transport along the partial barrier is slow, only its local, and not its global, flux is relevant for the dynamics of trapped orbits. Note that in a special 4D map, for which the relevant resonance channels are parallel to the surface of the regular region, the transport across resonance channels is the origin of the power-law trapping [57].

(iii.b) *Stochastic process with effective drift.*— The transport along a resonance channel is captured in Fig. 3(c). We conjecture that it can be modeled by a one-dimensional stochastic process with an effective drift: Such a drift was previously suggested due to the curvature of the regular tori [59, 60]. We propose that there is a much stronger and more general effective drift v due to the increase of the transversal 3D volume A along the resonance channel: Assuming a fast transversal diffusion one can project to a one-dimensional process along the channel with a phase-space coordinate x . According to the Fick-Jacob equation (Eq. (2.6) in Ref. [61]) this gives rise to a drift

$$v(x) = \frac{\partial_x A(x)}{A(x)} D(x) \quad (2)$$

with the local diffusion coefficient $D(x)$. The increase of the volume $A(x)$ along a channel is already visible in the

frequency space in Fig. 2(b) by the increasing widths of resonance channels going towards the chaotic region. Unfortunately, there is only weak numerical indication for such a drift so far, as the slow transport along a channel is very difficult to measure locally due to the lack of a sufficiently accurate one-dimensional coordinate x [57].

The transport along a resonance channel with an effective drift could be one mechanism of the power-law trapping: Assuming a power-law increase of the transversal volume along the channel $A(x) \sim x^\alpha$ and using $D(x) \sim A(x)$ [43] the drift is $v(x) = \delta x^{\alpha-1}$ with some factor δ , according to Eq. (2). For a process $x \in [0, x_{\text{abs}}]$ with an absorbing barrier at x_{abs} one can derive a power-law decay of the survival time distribution $P(t \gg 1) = t^{-\gamma}$ with $\gamma = \frac{\delta-1}{\alpha-2}$, $\alpha > 2$, $\delta > 1$, generalizing Ref. [62] to $\delta \neq \alpha$.

Outlook.— In this paper we advance towards understanding the mechanism of power-law trapping in generic 4D symplectic maps. The generality of the results is supported by similar observations we have made for coupled twist maps [57] and a 3D billiard [63]. It remains to be shown how the two local transport directions (across and along) of all the intersecting resonance channels determine the global transport. For this, (iii.a) the origin of the observed partial barriers should be clarified, i.e. whether they are families of cantori, and (iii.b) the drift and diffusion along channels should be quantified. Apart from the power-law trapping, the effective drift is crucial to understand the generic chaotic transport in the Arnold web. Since all higher-dimensional systems share the crucial property that regular tori are no barriers in phase space, the results obtained for 4D maps should be generalizable to even higher-dimensional systems.

We are grateful for discussions with J. D. Meiss, S. Keshavamurthy, J. Laskar, E. G. Altmann, M. Richter, M. Toda, H. Kantz, and R. Klages. Furthermore, we acknowledge support by the Deutsche Forschungsgemeinschaft under grant KE 537/6-1. All 3D visualizations were created using MAYAVI [64].

-
- [1] N. Murray and M. Holman, The role of chaotic resonances in the Solar System, *Nature* **410**, 773 (2001).
 - [2] P. M. Cincotta, Arnold diffusion: an overview through dynamical astronomy, *New Astron. Rev.* **46**, 13 (2002).
 - [3] J. Daquin, A. J. Rosengren, E. M. Alessi, F. Deleflie, G. B. Valsecchi, and A. Rossi, The dynamical structure of the MEO region: long-term stability, chaos, and transport, *Celest. Mech. Dyn. Astr.* **124**, 335 (2016).
 - [4] H. S. Dumas and J. Laskar, Global dynamics and long-time stability in Hamiltonian systems via numerical frequency analysis, *Phys. Rev. Lett.* **70**, 2975 (1993).
 - [5] M. N. Vrahatis, H. Isliker, and T. C. Bountis, Structure and breakdown of invariant tori in a 4-D mapping model of accelerator dynamics, *Int. J. Bifurcat. Chaos* **7**, 2707 (1997).
 - [6] D. Robin, C. Steier, J. Laskar, and L. Nadolski, Global dynamics of the advanced light source revealed through experimental frequency map analysis, *Phys. Rev. Lett.* **85**, 558 (2000).
 - [7] Y. Papaphilippou, Detecting chaos in particle accelerators through the frequency map analysis method, *Chaos* **24**, 024412 (2014).
 - [8] P. Schlagheck and A. Buchleitner, Algebraic decay of the survival probability in chaotic helium, *Phys. Rev. A* **63**, 024701 (2001).
 - [9] M. Toda, T. Komatsuzaki, T. Konishi, R. S. Berry, and S. A. Rice (editors) *Geometric Structures of Phase Space in Multidimensional Chaos: Applications to Chemical Reaction Dynamics in Complex Systems*, volume 130 of *Advances in Chemical Physics*, John Wiley & Sons, Inc.,

- Hoboken, New Jersey (2005).
- [10] S. Gekle, J. Main, T. Bartsch, and T. Uzer, Extracting multidimensional phase space topology from periodic orbits, *Phys. Rev. Lett.* **97**, 104101 (2006).
- [11] R. Paškauskas, C. Chandre, and T. Uzer, Dynamical bottlenecks to intramolecular energy flow, *Phys. Rev. Lett.* **100**, 083001 (2008).
- [12] H. Waalkens, R. Schubert, and S. Wiggins, Wigner's dynamical transition state theory in phase space: classical and quantum, *Nonlinearity* **21**, R1 (2008).
- [13] P. Manikandan and S. Keshavamurthy, Dynamical traps lead to the slowing down of intramolecular vibrational energy flow, *Proc. Natl. Acad. Sci. USA* **111**, 14354 (2014).
- [14] W. Bauer and G. F. Bertsch, Decay of ordered and chaotic systems, *Phys. Rev. Lett.* **65**, 2213 (1990).
- [15] M. Hirata, B. Saussol, and S. Vaienti, Statistics of return times: A general framework and new applications, *Commun. Math. Phys.* **206**, 33 (1999).
- [16] B. V. Chirikov and D. L. Shepelyansky, in *Proceedings of the IXth International Conference on Nonlinear Oscillations*, Kiev, 1981; [*Naukova Dumka* 2, 420 (1984)]; (English translation: Statistics of Poincaré recurrences and the structure of the stochastic layer of a nonlinear resonance, Princeton University Report No. PPPL-TRANS-133, 1983).
- [17] C. F. F. Karney, Long-time correlations in the stochastic regime, *Physica D* **8**, 360 (1983).
- [18] I. I. Shevchenko, Hamiltonian intermittency and Lévy flights in the three-body problem, *Phys. Rev. E* **81**, 066216 (2010).
- [19] G. S. Ezra, H. Waalkens, and S. Wiggins, Microcanonical rates, gap times, and phase space dividing surfaces, *J. Chem. Phys.* **130**, 164118 (2009).
- [20] A. K. Mazur and D. Shepelyansky, Algebraic statistics of Poincaré recurrences in a DNA molecule, *Phys. Rev. Lett.* **115**, 188104 (2015).
- [21] A. Sethi and S. Keshavamurthy, Driven coupled morse oscillators: visualizing the phase space and characterizing the transport, *Mol. Phys.* **110**, 717 (2012).
- [22] A. Buchleitner, D. Delande, J. Zakrzewski, R. N. Mantegna, M. Arndt, and H. Walther, Multiple time scales in the microwave ionization of Rydberg atoms, *Phys. Rev. Lett.* **75**, 3818 (1995).
- [23] G. Benenti, G. Casati, G. Maspero, and D. L. Shepelyansky, Quantum Poincaré recurrences for a hydrogen atom in a microwave field, *Phys. Rev. Lett.* **84**, 4088 (2000).
- [24] R. S. MacKay, J. D. Meiss, and I. C. Percival, Transport in Hamiltonian systems, *Physica D* **13**, 55 (1984).
- [25] J. D. Meiss and E. Ott, Markov-tree model of intrinsic transport in Hamiltonian systems, *Phys. Rev. Lett.* **55**, 2741 (1985).
- [26] V. Rom-Kedar and S. Wiggins, Transport in two-dimensional maps, *Arch. Rational Mech. Anal.* **109**, 239 (1990).
- [27] G. M. Zaslavsky, Chaos, fractional kinetics, and anomalous transport, *Phys. Rep.* **371**, 461 (2002).
- [28] M. Weiss, L. Hufnagel, and R. Ketzmerick, Can simple renormalization theories describe the trapping of chaotic trajectories in mixed systems?, *Phys. Rev. E* **67**, 046209 (2003).
- [29] G. Cristadoro and R. Ketzmerick, Universality of algebraic decays in Hamiltonian systems, *Phys. Rev. Lett.* **100**, 184101 (2008).
- [30] E. G. Altmann and T. Tél, Poincaré recurrences from the perspective of transient chaos, *Phys. Rev. Lett.* **100**, 174101 (2008).
- [31] R. Ceder and O. Agam, Fluctuations in the relaxation dynamics of mixed chaotic systems, *Phys. Rev. E* **87**, 012918 (2013).
- [32] O. Alus, S. Fishman, and J. D. Meiss, Statistics of the island-around-island hierarchy in Hamiltonian phase space, *Phys. Rev. E* **90**, 062923 (2014).
- [33] J. D. Meiss, Thirty years of turnstiles and transport, *Chaos* **25**, 097602 (2015).
- [34] See Supplemental Material at <http://www.comp-phys.tu-dresden.de/supp/> for videos with rotating camera position.
- [35] M. Ding, T. Bountis, and E. Ott, Algebraic escape in higher dimensional Hamiltonian systems, *Phys. Lett. A* **151**, 395 (1990).
- [36] E. G. Altmann and H. Kantz, Hypothesis of strong chaos and anomalous diffusion in coupled symplectic maps, *Europhys. Lett.* **78**, 10008 (2007).
- [37] A. Shojiguchi, C.-B. Li, T. Komatsuzaki, and M. Toda, Fractional behavior in multidimensional Hamiltonian systems describing reactions, *Phys. Rev. E* **76**, 056205 (2007), erratum *ibid.* **77**, 019902 (2008).
- [38] D. L. Shepelyansky, Poincaré recurrences in Hamiltonian systems with a few degrees of freedom, *Phys. Rev. E* **82**, 055202(R) (2010).
- [39] R. M. da Silva, C. Manchein, M. W. Beims, and E. G. Altmann, Characterizing weak chaos using time series of Lyapunov exponents, *Phys. Rev. E* **91**, 062907 (2015).
- [40] V. I. Arnol'd, Instability of dynamical systems with several degrees of freedom, *Sov. Math. Dokl.* **5**, 581 (1964).
- [41] B. V. Chirikov, A universal instability of many-dimensional oscillator systems, *Phys. Rep.* **52**, 263 (1979).
- [42] P. Lochak, Arnold diffusion; A compendium of remarks and questions, in C. Simó (editor) "Hamiltonian Systems with Three or More Degrees of Freedom", volume 533 of *NATO ASI Series: C - Mathematical and Physical Sciences*, 168, Kluwer Academic Publishers, Dordrecht (1999).
- [43] B. P. Wood, A. J. Lichtenberg, and M. A. Lieberman, Arnold diffusion in weakly coupled standard maps, *Phys. Rev. A* **42**, 5885 (1990).
- [44] J. Laskar, Frequency analysis for multi-dimensional systems. Global dynamics and diffusion, *Physica D* **67**, 257 (1993).
- [45] M. Guzzo, E. Lega, and C. Froeschlé, First numerical evidence of global Arnold diffusion in quasi-integrable systems, *Discrete Contin. Dyn. Sys. Ser. B* **5**, 687 (2005).
- [46] M. Guzzo and E. Lega, The numerical detection of the Arnold web and its use for long-term diffusion studies in conservative and weakly dissipative systems, *Chaos* **23**, 023124 (2013).
- [47] C. Efthymiopoulos and M. Harsoula, The speed of Arnold diffusion, *Physica D* **251**, 19 (2013).
- [48] M. F. Mestre, A. Bazzani, P. M. Cincotta, and C. M. Giordano, Stochastic approach to diffusion inside the chaotic layer of a resonance, *Phys. Rev. E* **89**, 012911 (2014).
- [49] C. C. Martens, M. J. Davis, and G. S. Ezra, Local frequency analysis of chaotic motion in multidimensional systems: energy transport and bottlenecks in planar OCS, *Chem. Phys. Lett.* **142**, 519 (1987).
- [50] S. Wiggins, On the geometry of transport in phase

- space I. Transport in k -degree-of-freedom Hamiltonian systems, $2 \leq k < \infty$, *Physica D* **44**, 471 (1990).
- [51] R. S. MacKay and J. D. Meiss, Cantori for symplectic maps near the anti-integrable limit, *Nonlinearity* **5**, 149 (1992).
- [52] C. Froeschlé, Numerical study of a four-dimensional mapping, *Astron. & Astrophys.* **16**, 172 (1972).
- [53] M. Richter, S. Lange, A. Bäcker, and R. Ketzmerick, Visualization and comparison of classical structures and quantum states of four-dimensional maps, *Phys. Rev. E* **89**, 022902 (2014).
- [54] S. Lange, M. Richter, F. Onken, A. Bäcker, and R. Ketzmerick, Global structure of regular tori in a generic 4D symplectic map, *Chaos* **24**, 024409 (2014).
- [55] J. Laskar, The chaotic motion of the solar system: A numerical estimate of the size of the chaotic zones, *Icarus* **88**, 266 (1990).
- [56] R. Bartolini, A. Bazzani, M. Giovannozzi, W. Scandale, and E. Todesco, Tune evaluation in simulations and experiments, *Part. Accel.* **52**, 147 (1996).
- [57] S. Lange, *Chaotic transport and trapping close to regular structures in 4D symplectic maps*, Ph.D. thesis, Technische Universität Dresden, Fachrichtung Physik (2016).
- [58] F. Onken, S. Lange, R. Ketzmerick, and A. Bäcker, Bifurcations of families of 1D-tori in 4D symplectic maps, *Chaos* **26**, 063124 (2016).
- [59] A. Kruscha, R. Ketzmerick, and H. Kantz, Biased diffusion inside regular islands under random symplectic perturbations, *Phys. Rev. E* **85**, 066210 (2012).
- [60] O. Castejón and V. Kaloshin, Random iteration of maps on a cylinder and diffusive behavior, arXiv:1501.03319 [math.DS] (2015).
- [61] P. Kalinay and J. K. Percus, Projection of two-dimensional diffusion in a narrow channel onto the longitudinal dimension, *J. Chem. Phys.* **122**, 204701 (2005).
- [62] A. E. Motter, A. P. S. de Moura, C. Grebogi, and H. Kantz, Effective dynamics in Hamiltonian systems with mixed phase space, *Phys. Rev. E* **71**, 036215 (2005).
- [63] M. Firmbach, *3D Billards: Dynamik im gemischten Phasenraum und Potenzgesetz des Hängenbleibens*, Bachelor thesis, Technische Universität Dresden, Fachrichtung Physik (2014).
- [64] P. Ramachandran and G. Varoquaux, Mayavi: 3D visualization of scientific data, *Comput. Sci. Eng.* **13**, 40 (2011).